Design and Analysis of a Cable-winding Device for Cable Suspended Parallel Robot

Nguyen Minh Trieu and Nguyen Truong Thinh*

College of Technology and Design, University of Economics Ho Chi Minh City–UEH University, Vietnam
Email: trieunm@ueh.edu.vn (N.M.T.)
*Correspondence: thinhnt@ueh.edu.vn (N.T.T.)

***Abstract*—Cable-Driven Parallel Robots (CDPR) have recently been applied in a variety of industries. Particularly in specialized industrial fields where dynamic features such as high precision in systems demand quick transitions so that cable-driven parallel robots have been deployed. The cable force is the most important factor influencing the control algorithm of the cable-suspended parallel robot. The cable force at the attachment point of the cables at the platform and the winch are different. Due to friction, the pulleys between the force sensor and the platform affect the force measurement accuracy. This disparity is caused by a variety of factors, including high acceleration, stiffness, cable density, and cable length. In this paper, a dynamic model and cable tension are designed for cable transmission to increase the accuracy of cable forces. The influencing variables of the cable force during motion are defined by studying the force relationship of the cable. Finally, experiment and numerical simulation are used to verify the correctness of the research content in this study. The results show that the model can accurately simulate the force state of the cable compared to the actual force measured at the load cell.**

***Keywords*—Cable Robot, Cable-Driven Parallel Robots (CDPR), kinematics, cable winding, cable tension**

I. Introduction

In recent decades, robots are increasingly popular for many applications in various fields such as medicine, agriculture, construction, etc [1–4]. Furthermore, robotic mechanisms have been used to manipulate objects within a workspace. Conventional robots with serial are impractical for long-reach robotics, such as inspection and repair at shipyards and airplane hangars, since the workspace requirements are larger than what conventional robots can provide. Cable-driven mechanisms have gotten a lot of attention because of these issues, and they've lately been researched: high-speed robots, aerial camera systems, multidimensional cranes, Robocrane [5] are just a few examples of the most recent research on lightweight cable suspended robots that can work in a variety of workplaces. Besides, there are many cable robot studies for different applications [6–9].

Manuscript received April 20, 2023; revised July 24, 2023; accepted August 27, 2023.

The cable robots are powered by motors that wind or unwind the cables from pulleys to extend or retract them (also called winches or drums). When compared to traditional serial and parallel robots, cable robots have a lot of benefits. They have thus been extensively studied and have the potential to significantly improve the payload, workspace, and dynamic performances of today's industrial robots. They can be designed to have a very large workspace, a very high load capacity, or to generate very high-speed motions, always with a significant amount of energy efficiency. As a result, a technique must be defined to transform the intended cable tension into a variable that the motor drivers can understand, such as motor torque (or current), position, or velocity. Cable tension control systems are a type of control strategy. An open-loop cable tension control is used in most published test findings.

In the framework of position tracking control [10] and control-based force [11], a frequent approach is to apply the torque of a friction-compensating motor in the winch [12–14]. Nonetheless, using a closed-loop technique significantly improves the stability of the controlled system. Closed-loop cable tension control is a simplified case of feedback force control, which is a well-known issue in robotics [15]. Impedance control [16] and hybrid position/force are two examples of its derivatives.

The rest of the paper is structured as follows: Section II is the inverse kinematics Model. Section III is the design of the cable-winding device. Section IV is the Overview of the cable winch. Section V is the pulley friction model. Section VI is the test trajectory and experiment. Section VII concludes with a conclusion and vision on future works.

II. Inverse Kinematics Model

A description of the inverse kinematics problem is to find the positions of the motor (q_i, i= 1, 2..., n) that meet the static equilibrium and geometry requirements given a specified payload position and orientation (p, R). The platform requires three coordinates to identify its position in 3–D space. Vector L_i is the point from Bi to Ai, the ith cable vector, and reads as Eq. (1).

$$^{b}\boldsymbol{L}_i = l_i \boldsymbol{u}_i = {}^{b}\boldsymbol{a}_i - {}^{b}\boldsymbol{r} - {}^{b}\boldsymbol{R}_p \, {}^{P}\boldsymbol{b}_i \quad (1)$$

doi: 10.18178/ijmerr.12.5.332-338

Where: F_b is the movement platform frame. The position vector point from O to A_i is shown in frame F_b; the position vector B_i point from P to B_i is shown in frame F_b; corresponds to the rotation matrix from F_b to frame F_p, ui is the unit of the cable vector.

$$l_i = \left\| {}^{b}L_i \right\|^2 \text{ and } {}^{b}u_i = \frac{{}^{b}l_i}{\left\| {}^{b}L_i \right\|^2} \tag{2}$$

where $\| . \|$ denotes the Euclidean norm of a vector.

The rotation matrix R from F_b to frame F_p can be obtained as follows:

$${}^{b}R_P = \begin{bmatrix} c\alpha c\beta & c\alpha c\beta s\gamma - s\alpha c\gamma & c\alpha s\beta c\gamma + s\alpha s\gamma \\ s\alpha c\beta & s\alpha s\beta s\gamma - c\alpha c\gamma & s\alpha s\beta c\gamma + c\alpha s\gamma \\ -s\beta & c\beta s\gamma & c\beta c\gamma \end{bmatrix} \tag{3}$$

In Eq. (3), c indicates cos and s indicates sin. Also α, β, and γ are angles of rotation around z, y and x axis respectively. Below equation shows the relationship between kinetics, statics and dynamics of CDPR.

The issue with CDPRS kinematics is that controlling the location or force of the moving base of the CDPRs is insufficient. The cables can only provide pulling forces, rather than pushing forces. The cable tension has a significant impact on the CDPMs' determination workspace. The cable tension has a significant impact on the determination workspace for CDPMs [17]. demonstrates that the cables create tension forces to balance any external wrench (Fp, Mp) applied to a moving platform, resulting in platform equilibrium. The following equilibrium equations may be utilized to calculate the forces and torques operating on the CDPRs:

$$W\tau + w_g = 0 \tag{4}$$

W is the wrench matrix of the robot and expressed as

$$W = \begin{bmatrix} {}^{b}u_1 & \cdots & {}^{b}u_m \\ {}^{b}b_1 \times {}^{b}u_1 & \cdots & {}^{b}b_1 \times {}^{b}u_m \end{bmatrix} \tag{5}$$

τ is the cable tension vector. w_g is vectors of the external wrenches applied to the mobile platform's center of mass. For CDPRs, the forward Jacobian matrix A relates the movement platform twist v and the cable unwinding velocities:

$$A\xi = \dot{l} = \frac{r_\omega}{R}\dot{q} = \dot{l} \text{ with } \xi = \begin{bmatrix} {}^{b}\dot{v} & {}^{b}\omega \end{bmatrix}^T \tag{6}$$

$\dot{l} = \begin{bmatrix} \dot{l}_1 & \cdots & \dot{l}_s \end{bmatrix}^T$ is the vector containing the cable velocities, $\dot{q} = \begin{bmatrix} \dot{q}_1 & \cdots & \dot{q}_8 \end{bmatrix}^T$ is the vector containing the motor velocities. where R is the gearbox reduction ratio, r_w is the winch radius. ${}^{b}\omega$ is the angular velocity. ${}^{b}\dot{V}$ is the Cartesian position of movement platform. ξ is the vector end effector velocities. The relationship between the kinematics, statics and dynamic can be written as Eq. (7). From Eq. (8), the calculation of the transmission design is based on the speed and tension of the cable.

$$W = -A^T \tag{7}$$

$$A\tau + \omega_p = 0 \tag{8}$$

Because A is not square, this issue can be solved by using a pseudo-inverse matrix. Pseudo-inverse matrix, linear programming, interval analysis, and other techniques can be used to evaluate if an inequality equation has a solution or not.

The dynamic model of the CDPR can be written as

$$Wt - I_p\dot{\zeta} - C\zeta + w_e + w_g = 0 \tag{9}$$

where I_p is the spatial inertia of the platform. C is the matrix of the centrifugal and Coriolis wrenches. The wrench w_g due to the gravity acceleration g. we is an external wrench. However, because the platform is moving at a low speed in this experiment, Coriolis and external wrenches may be ignored.

Figure 1. Cable Robot with 8 cables, 6 dof.

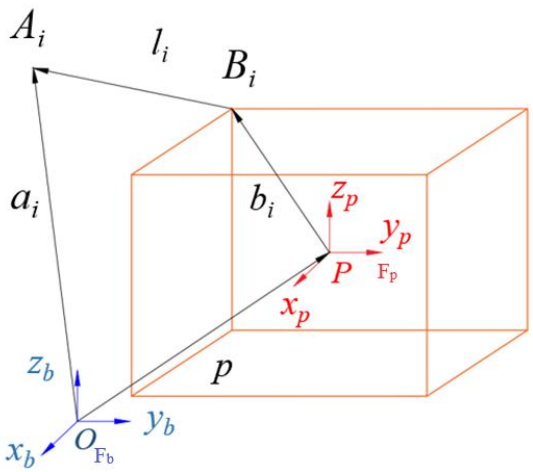

Figure 2. The robot kinematic.

III. Design of the Cable-winding Device

Cable wrapping equipment has to meet specifications for functions like wrapping and unwrapping as well as working circumstances in construction:

- Large driving force: The ability to resist the gravity of the movement platform. The primary purpose of the winding device is to provide a substantial driving force in order to let the movement of the mechanism to be launched.

- Large displacement of cable: The variation in the length of the drive cable is quite large so the equipment designed to wind the cable must be uniform.
- Compactness: To preserve machine space, the device's geometric structure should take up a minimum amount of area.

To fulfill the above-mentioned design criteria, the cable reel is designed equipment consisting of three parts: the transmission assembly (which offers high dynamics to actuate the mechanism), the cable arrangement assembly (which assures the right cable reel on the winch), and spare engine assembly (which improves equipment reliability)

A. Selecting Motor for System

It is important to compute the motor selection for each section of the cable robot in order to assist it to operate and being steady. Because it is an open-loop system, choosing a motor for a series-type robot is very simple. Because selecting motors for parallel robots is more challenging due to the closed-loop control system, CDPR is divided into four parts (each pillar is a part) that can be divided into four separate series sections, each of which utilizes a gear reducer connected in series with the motor.

The efficiency of the transmission assembly is

$$\eta_{hs} = \eta_{ol}{}^2 \cdot \eta_d{}^2 \cdot \eta_{gt} \tag{10}$$

where η_d are the efficiencies of belt-drive transmission, the pair of gearbox, the pair of roller bearing η_{ol} = 0.99, η_d = 0.95, η = 0.8, respectively.

The motor's output power, which is calculated as

$$P = \frac{P_t}{\eta_{hs}} = \frac{F_g \cdot v}{\eta_{hs}} = \frac{m \cdot g \cdot v}{\eta_{hs}} \tag{11}$$

where m is the maximum mass of the movement platform is the desired control speed, g is the gravity acceleration with the efficient η_{hs} = 0.68. The parameters of Table I are substituted into (10) to derive the value of P, which is 80 W. Considering the margin of the motor, a motor with a capacity of 400 W, accompanied by a 1:30 gearbox, is considered, based on the characteristics of AC servo motors offered by brands ranging from 100 W to 7.5 kW. After the motor has been determined, the parameters of the winch, the reductor can be calculated.

B. Design of a Cable Winch

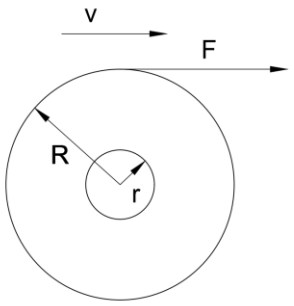

Figure 3. Force wrapped on the winch.

TABLE I. DRIVING REQUIREMENTS

Item	F_g	V	L_w	v_m
Value	1000 N	0.05 m/s	20 m	0.5 cm/s

As shown in Fig. 3, the radius of the winch is rw when there is no cable wound, and the radius is R_w when the cable, whose length is L_w is wound. The radius of the cable is r_c; b is the width of each groove on the reel. Number of turns of cable required to get 20 (*m)*. B is the length of the winch can be written as:

$$B = N \times b = \frac{L_w}{2\pi(r_w + r_c)} \times b \tag{12}$$

The parameters of Table I are substituted into (10) to derive the value of B, which is 300 (mm).The torque and rotation speed of the motor's output shaft should be less than the rated torque and speed of revolution in order to guarantee smooth operation. The torque of the winch increases while the cable force remains constant, and it reaches its maximum value when the cable is entirely wrapped around the winch. When the cable's velocity remains constant, the motor's rotation speed decreases as the cable is wrapped. As a result, the motor's rotational speed and torque restrictions are stated as:

$$\begin{cases} \dfrac{F_g R}{\eta_{hs} u_t} \le \tau_0 \\ \dfrac{v u_t}{\pi r} \le n_0 \end{cases} \tag{13}$$

where η_o is the reduction ratio of transmission assembly. Driving the winch directly from the motor is unable, thus an appropriate reducer to increase the winch's torque is necessary. Furthermore, the use of a reducer will lower the robot's speed to some amount, but it will be simpler to regulate and avoid a large reaction that acts directly on the motor, assuring the robot's safety and the operating life of motor. The motor can be mounted directly for spindle movement, but we need a gear reducer to assure the motor's safety.

$$u_t = \frac{n_1}{n_2} = \frac{z_2}{z_1} \tag{14}$$

where: z_1 is the number of teeth in the worm gear, z_2 is the number of screw thread and n_1; n_2 are the numbers of revolution of screw gear and worm thread. From Eq. (11), the selected reducer is NMRV 050 (gear ratio 1/30)

C. Loadcell and Cable Guide

A cable winder, as shown in Fig. 6, with a loadcell sensor that monitors the tension of the cable, is used to keep the cables from becoming tangled while winding. A guide includes: a screw rod with a diameter of 20 mm with a step of 5 mm, two 16 mm diameter guide rails, a lead screw nut holder, a guide bar nut, and a loadcell are included with the guide (200 kg). The step of the lead screw as Eq. (15).

$$l_m \geq \frac{v_m}{N_{dc}} \tag{15}$$

where: v_m is maximum speed without load, N is the revolution of the motor. L_m is the max total displacement length and the length of nut and bearing, which is 730 mm Ball bearing type is tight fitting at both ends f = 21.9. The rotation speed for the motor is selected at about 80% compared to the limited rotation speed, so n = 80% and Nmax = 3600 rpm. The radius of the lead screw can be written as

$$r_v = \frac{nL_m}{f} \cdot 10^{-7} \tag{16}$$

D. Tooth Belt Drive

The lead screw rod has a tooth pitch of p_1 = 5, and the under step on the cable reel p_2 = 5 so we choose the gear ratio k = 1. The width of the belt can be written as:

$$m = 35\sqrt[3]{\frac{P_{b1}}{N_{b1}}} \tag{17}$$

where m is module; P is power on the drive pulley; N is the number of revolutions on the drive wheel. According to the standard tooth width table [2] corresponding to m = 1.5. The belt width b = 16 (*mm*) is suitable for the proposed condition. With the tooth width b = 16, the number of teeth needed for the pulley is from 30 teeth to 40 teeth. Calculation of belt length:

$$A = \frac{1}{4} \times \left[\begin{array}{l} L_d - \pi\left(R_1 + R_2\right) \\ + \sqrt{L - \pi\left(R_1 + R_2\right)^2 - 8\left(R_1 + R_2\right)^2} \end{array} \right] \tag{18}$$

where A is the shaft distance, L_d is the belt length and R_1, R_2 is the pulley radius 1, 2, respectively.

From Eq. (18) we can define the length of the belt. The existence of a mechanical part that serves as a static limitation on the cable is generally the origin of any forward static friction between the released cable and the force sensor; these forces cannot be measured directly at the winch since they are not visible at the force sensor. In fact, without additional information on the applied forces provided by the force sensor in the Coulomb static friction mode, they cannot be adjusted via an open-loop technique. However, dynamic forward friction can be included after calculating the associated Coulomb coefficient, which is the displacement of the force contact point between a cable and the force sensor.

IV. Overview of the Cable Winch

The winch is the winding part in the lifting machine, which converts the rotational motion into the reciprocating motion of lifting and lowering the platform movement. The characteristics are shown like that:

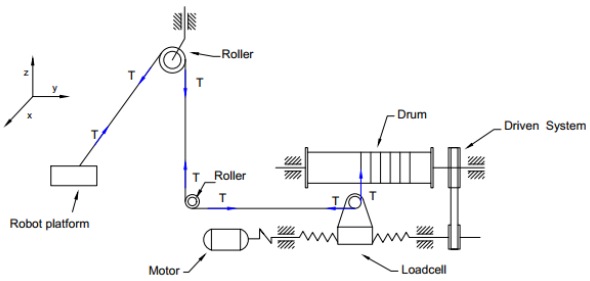

Figure 4. Schematic of cable winch.

- The drum is usually cylindrical in shape, with holes at both ends for mounting with the shaft, rotating movement.
- Material of the drum: steel.
- The working surface cut into a circular threaded groove with a step larger than the cable diameter to avoid the cables rubbing against each other (grooved drum).
- Reel winch can be used to wind multiple layers of cable overlap.

Design of cable drum winch, diameter 100mm, shaft diameter 25 mm using UCF bearing with 25 mm inner diameter with design as shown in Fig 4. In addition, the pulleys to guiding the cable winding on the winch are designed uniformly in order to avoid cable tangles so that the cable wraps around the drum right at the pre-designed groove. The cable guide set includes: 2 chrome-plated steel smooth rods to help orient and increase the stiffness of the drum, 1 lead screw to guide the cable into the designed groove, 1 connecting detail between the 2 rods, slide and lead screw bar, and install a loadcell measuring the cable tension to avoid overloading leading to cable breakage. The guide is driven through a belt mechanism located at the end of the drum as shown in Fig 5.

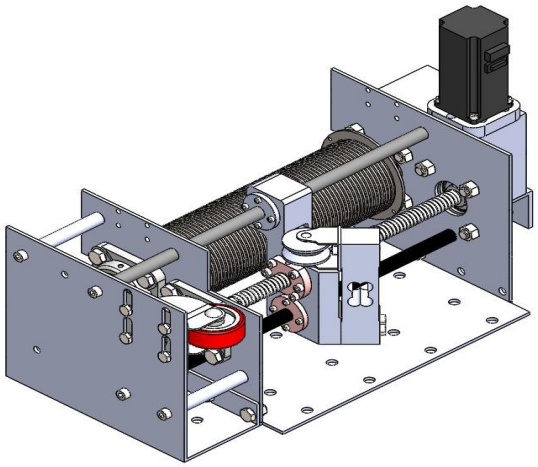

Figure 5. 3D model of the designed device.

V. Pulley Friction Model

Whenever pulleys or cables are designed, it is important to define the friction forces contacting surface between them. To determine the tension T_j, which is necessary to pull the belt counter-clockwise. Euler-Eytelwein equation

with kinetic friction between the surface of pulley and cable, wrapping angle ai in of the i^{th} pulley, p is the friction coefficient. The schematic of a pulley system is shown in Fig. 6.

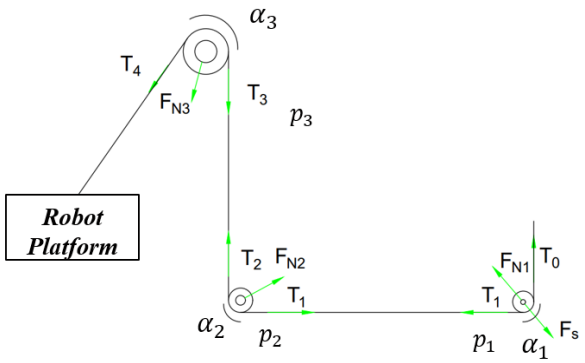

Figure 6. The guide of three pulleys for a cable.

$$T_j = T_{j-1} e^{\mu_P \alpha} \tag{19}$$

The cable's elasticity and gravity are ignored. In the case of force equilibrium, a force Fr is acting to guide the pulley with velocity v in the same direction as T_j, as defined by below equation.

$$T_j = T_{j-1} + \mathrm{sgn}(v) F_{R,j} \tag{20}$$

T_j, T_{j-1} is the tension before and after the pulley. The pulley's friction force is determined by Coulomb coefficient of friction and viscous friction parameter F_{pv}.

$$F_{Rj} = \mu_i F_{N,j} + F_{pv} |v| \tag{21}$$

where: $F_{N,j}$ is the normal force to pulley j^{th}.

It is possible to determine the normal force from both the first and second tensions applied to the pulley by the cosine law. The Coulomb friction in the static model can be described as follows.

$$F_{N,j} = \sqrt{T_{j-1}^2 - 2T_{j-1}T_j \cos \infty_j + T_j^2} \tag{22}$$

$$F_{Rj} = \mu_j F_{N,j} \tag{23}$$

For greater precision, both Coulomb and viscous friction should be considered. The viscous impact is too minimal because our CDPR system operates at a speed of less than 10 m/s. As a result, viscous friction is omitted in this analysis. We can also regulate the pose by taking use of the Coulomb friction term's simplicity.

$$F_{N,j} = \sqrt{T_{j-1}^2 - 2T_{j-1}T_j \cos \infty_j + T_j^2}$$

$$\sum_{j=1}^{3} F_{Rj} = \sum_{j=1}^{3} \prod_{k=1}^{3-j} n_k \left[\mu_j \cdot \sqrt{n_3^2 - 2n_{3+1-j} \cos(\alpha_j) + 1} \right] T_1 \tag{24}$$

Coulomb friction, on the other hand, has limitations is that it ignores pre-sliding dynamics at low velocities. Dahl friction can be used to model the pre-sliding dynamics. These dynamics are nonlinear when the velocity is close to zero. The Dahl friction first-order non-linear ordinary differential equation is presented. The Dahl friction model can be expressed in the following way [18, 19].

$$\frac{dF_{d,j}(T_j)}{dx} = \sigma \left[1 - \frac{F_{d,j}(T_j)}{F_{Rj}} \mathrm{sgn}(v) \right]^{\beta} \tag{25}$$

$$F_{d,j}(T_j) = F_{Rj}(1 - e^{-\frac{\sigma |x|}{F_{Rj}}}) \mathrm{sgn}(v) \tag{26}$$

By simplifying the model with an exponential function α=1, F_{Rj} is the maximum value of the friction force. The problem with the linear Dahl model is that the exponential function is related to position and represents the zero slope across the graph. $F_{d,j}$ is the Dahl friction of j^{th} pulley, σ represents the slope of the friction with respect to position at the zero crossing, that determine the pre-sliding range, x is the relative displacement between the cable and the pulley, and β define the pre-sliding shape and takes the value β = 1.1[4.26] in most cases. Decoupling tension and friction factors can be utilized to generate a value for the tension that includes Dahl friction because Dahl friction is a function of Coulomb friction. Two of these factors are the loss factor and the friction coefficient. By incorporating equation, Eq. (5) for kinematics and dynamics may be enlarged. The Dahl model is part of a modified version of the kinematics equation, which is written as:

$$T + \sum_{j=1}^{3} \left[1 - e^{\frac{-\sigma |x|}{\lambda_j T}} \right] \lambda_j \mathrm{sgn}(v) T = [A]^{+} \omega_p \tag{27}$$

VI. Performance of Cable Force Transmission

The cable force at the winch is the actual force measured by the force sensor. The desired force and the actual force are almost similar when the terminal acceleration is very small. The first significant assessment indicator is cable overshoot, which measures the highest departure of cable force from the desired force. The following is the expression:

$$\sigma = \frac{F(t_m) - F_O}{F_O} \times 100\% \tag{28}$$

The target force is specified as F_O, while the moment when the actual cable force is at its greatest is defined as tm. The average relative error is ε , defined as follows:

$$\varepsilon = \frac{1}{n} \sum_{i=1}^{i=n} \left| \frac{F(t) - F_O}{F_O} \right| \times 100\% \tag{29}$$

We evaluate the error conditions in the cable-force transmission process using the average relative error ε in Eq. (29).

VII. Test Trajectory and Experimental Setup

A CDPR is used for experimental cases with system's parameters (Table II). A desired trajectory representing a

typical motion simulation application has been built to assess the efficacy of alternative control techniques. S-curves are used to create the trajectory, which ensures that the velocity and acceleration profiles are consistent. The frame F_b has an x-axis that runs the length of the CDPR, a y-axis that runs the length of the CDPR, and a z-axis that runs the height of the CDPR. The XY trajectory has a 400x430 mm rectangle edge and is meant to move the objects which is shown in Fig.7.

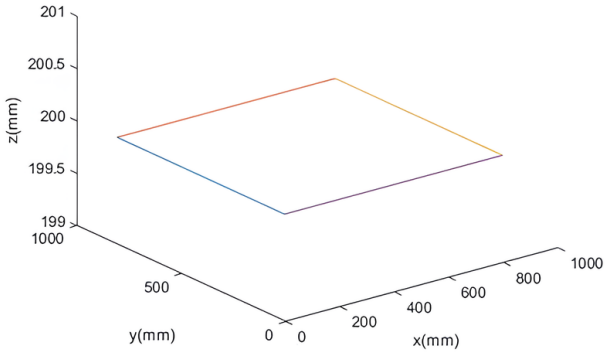

Figure 7. Rectangle trajectory with Z = 200mm.

TABLE II. CDPR SPECIFICATION FOR EXPERIMENTS

Specification	Value
Degree of Freedom	6
Number of cables	8
Size structure	6000 ×6000 ×1200 mm
Maximum load	250 kg
Minimum load 40 kg	40 kg
Moving velocity (Vp)	0.05 m/s
Applied voltage	200–300 V, 50–60 Hz
Power of motor	400W

In the case of low speed, Fig. 8 shows the tension data collected experimentally and through simulations. The orange line is the tension profile that was the target force and blue lines represent the tension profiles that were measured. With the Dahl friction model, the inaccuracy throughout the whole range of motion was greatly reduced. The total error was computed across the completed range of movement. The mean and standard deviation of the error for Dahl models were 17.9 and 20.5 N, respectively. The Dahl friction is more precise at low speeds. If the system requires high positioning precision and many movement transitions, pre-sliding is the most important component of the dynamics in addition, the error due to noise of the sensor is read. Factors affecting the error include the production tolerance of the loadcell, the impact of the air on the axial suspension. In general, the actual tension measured at the force sensor and the desired force is up to 96% similar to the original desired condition. From the comparison of the string tension including the friction compensation, it can be concluded that the cable drive is relatively stable in accordance with the tension requirement.

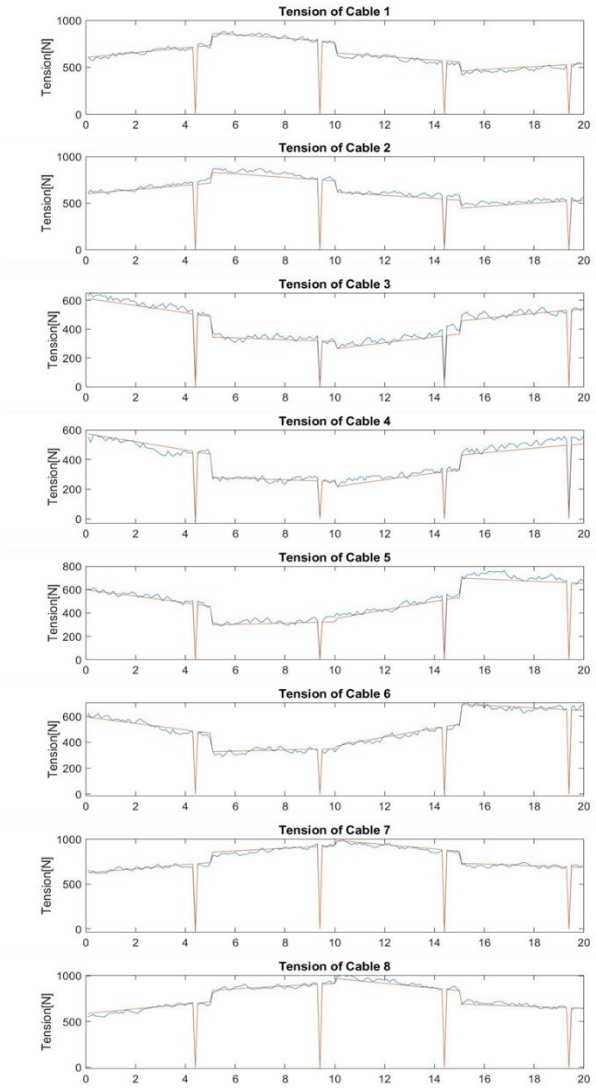

Figure 8. Describe tension data profiles in the case of low-speed

VIII. CONCLUSIONS

This paper presents a cable-winding mechanism that can generate a large cable-driving force, organize the cable uniformly and achieve high dependability. The device fulfills the required specifications. The transmission assembly converts the motor's high speed and low torque into the cable's supplied speed and high driving force. The minimum cable tension limit expresses the need that the cable be maintained tight. The maximum cable tension is mostly determined by the greatest load that may be safely applied to the robot's mechanical components. An internal cable tension feedback control loop in which the desired tension is the MPC's output. This is a strategy that is not based on a motor velocity control model that is a proposal for future research.

CONFLICT OF INTEREST

The authors declare no conflict of interest.

AUTHOR CONTRIBUTIONS

Nguyen Minh Trieu is the first author-methodology, wring–original draft, visualization, validation, configured; Nguyen Truong Thinh is correspondent, writing–review and editing, methodology, project administration.

ACKNOWLEDGMENT

This research is funded by University of Economics Ho Chi Minh City–UEH University, Vietnam.

REFERENCES

[1] J. Zhang, J. Wang, S. Dong, X. Yu, & B. Han, "A review of the current progress and application of 3D printed concrete," *Composites Part A: Applied Science and Manufacturing*, vol. 125, 2019, 105533.

[2] S. Bhooshan, J. Ladinig, T. Van Mele, and P. Block, "Function representation for robotic 3D printed concrete," In Robotic Fabrication in Architecture, Art and Design 2018: Foreword by Sigrid Brell-Çokcan and Johannes Braumann, Association for Robots in Architecture (pp. 98-109). Springer International Publishing, 2019.

[3] N. H. Vu, N. M. Trieu, H. N. Anh Tuan, T. D. Khoa, and N. T. Thinh, "Facial anthropometric, landmark extraction, and nasal reconstruction technology," *Applied Sciences*, vol. 12, no. 19, 9548, 2022.

[4] N. M. Trieu and N. T. Thinh, "Quality classification of dragon fruits based on external performance using a convolutional neural network," Applied Sciences, vol. 11, no. 22, 10558, 2021.

[5] R Bostelman, J Albus, N Dagalakis, A Jacoff, J Gross, "Applications of the NIST RoboCrane," in *Proc. of the 5th International Symposium on Robotics and Manufacturing*, 1994.

[6] T. P. Tho and N. T. Thinh, "Using a cable-driven parallel robot with applications in 3D concrete printing," *Applied Sciences*, vol. 11, no. 2, p. 563, 2021.

[7] T. Bruckmann and R. Boumann, "Simulation and optimization of automated masonry construction using cable robots," *Advanced Engineering Informatics*, vol. 50, 101388, 2021.

[8] T. T. P. Thanh and N. T. Thinh, "Winch-integrated cable force measurement and verification on driven cable parallel robot 6 DoF," *International Journal of Mechanical Engineering and Robotics Research*, vol. 11, no. 10, 2022.

[9] P. G. Luan and N. T. Thinh, "Overconstrained cable-driven parallel manipulators statics analysis based on simplified static cable model," *International Journal of Mechanical Engineering and Robotics Research*, vol. 11, no. 3, pp. 159-165, March 2022.

[10] T. Higuchi, "Application of multi-dimensional wire crane in construction," in *Proc. 5th Int. Symp. on Robotics in Construction*, 1988.

[11] N. Hogan, "Impedance control: An approach to manipulation," in *Proc. 1984 American Control Conference*, 1984, pp. 304-313.

[12] T. Higuchi, "Application of multi-dimensional wire crane in construction," in *Proc. 5th Int. Symp. on Robotics in Construction*, 1988.

[13] P. Etienne, et al., "A new control scheme of cable-driven parallel robot balancing between sliding mode and linear feedback," *IFAC-Papers Online*, vol. 53, no. 2, pp. 9936-9943, 2020.

[14] K. Werner, *et al*., "Hybrid position-force control of a cable-driven parallel robot with experimental evaluation," *Mechanical Sciences*, vol. 6, no. 2, pp. 119-125, 2015.

[15] JC Santos, A Chemori, M Gouttefarde, "Redundancy resolution integrated model predictive control of cdprs: concept, implementation and experiments," in *Proc. 2020 IEEE International Conference on Robotics and Automation (ICRA)*, 2020, pp. 3889-3895.

[16] H. Neville, "Impedance control: An approach to manipulation," in *Proc. 1984 American Control Conference*, IEEE, 1984, pp. 304-313.

[17] K. Wang, et al. "CDPM: Convolutional deformable part models for semantically aligned person re-identification," *IEEE Transactions on Image Processing*, vol. 29, pp. 3416-3428, 2019.

[18] D. A. Haessig Jr and B. Friedland, "On the modeling and simulation of friction," *Journal of Dynamic Systems, Measurement, and Control*, vol. 113, no. 3, pp. 354-362, 1991.

[19] L. D. Duy and N. T. Thinh, "Dynamic modeling of a cable suspended parallel robot," *International Journal of Mechanical Engineering and Robotics Research*, vol. 11, no. 8, pp. 639-645, August 2022, 2022.